Available online at www.sciencedirect.com

ScienceDirect

Green Energy & Environment xxx (xxxx) xxx

www.keaipublishing.com/gee

Research Paper

Ammonia-induced CuO/13X for H_2S removal from simulated blast furnace gas at low temperature

Erping Cao [a], Yuhua Zheng [a], Hao Zhang [a], Jianshan Wang [b], Yuran Li [a], Tingyu Zhu [a], Zhan-guo Zhang [c,*], Guangwen Xu [c], Yanbin Cui [a,*]

[a] State Key Laboratory of Mesoscience and Engineering, Institute of Process Engineering, Chinese Academy of Sciences, Beijing, 100190, China
[b] State Key Laboratory of Vanadium and Titanium Resources Comprehensive Utilization, PanGang Group Research Institute Co., Ltd., Panzhihua Sichuan, 617000, China
[c] Shenyang University of Chemical Technology, Shenyang, 110142, China

Received 7 December 2023; revised 30 January 2024; accepted 3 February 2024
Available online ■ ■ ■

Abstract

Blast furnace gas (BFG) is an important by-product energy for the iron and steel industry and has been widely used for heating or electricity generation. However, the undesirable contaminants in BFG (especially H_2S) generate harmful environmental emissions. The desulfurization of BFG is urgent for integrated steel plants due to the stringent ultra-low emission standards. Compared with other desulfurization materials, zeolite-based adsorbents represent a viable option with low costs and long service life. In this study, an ammonia-induced CuO modified 13X adsorbent (NH_3–CuO/13X) was prepared for H_2S removal from simulated BFG at low temperature. The XRD, H_2-TPR and TEM analysis proved that smaller CuO particles were formed and the dispersion of Cu on the surface of 13X zeolite was improved via the induction of ammonia. Evaluation on H_2S adsorption performance of the adsorbent was carried out using simulated BFG, and the results showed that NH_3–CuO/13X-3 has better breakthrough sulfur capacity, which was more than twice the sulfur capacity of CuO/13X. It is proposed that the enhanced desulfurization performance of NH_3–CuO/13X is attributed to an abundant pore of 13X, and combined action of 13X and CuO. This work provided an effective way to improve the sulfur capacity of zeolite-based adsorbents via impregnation method by ammonia induction.

Keywords: Blast furnace gas; Desulfurization; Ammonia-induced; CuO; 13X zeolite

1. Introduction

Blast furnace gas (BFG) from iron and steel enterprises is an important source of energy and used mainly for heating and electricity generation [1,2]. The volume of BFG in integrated steel plants is very huge and 1200–2000 Nm^3 of BFG will produce per ton of metal. However, BFG also contains various pollutants (including sulfur compounds) and generates harmful environmental emissions, which hinder its utilization. The total sulfur content in BFG typically ranges from 100 to 200 mg Nm^{-3}. Carbonyl sulfide (COS) and hydrogen sulfide (H_2S) are the main sulfur components, accounting for 70% and 30%, respectively [3]. These sulfides in BFG can cause corrosion of industrial equipment, poisoning of catalysts, or environmental pollution [4–6]. COS emission into atmosphere can form SO_2 and accelerate photochemical reaction, which will transform into sulfate aerosols finally. Therefore, effective desulfurization of BFG is of great significance for iron and steel companies. Compared with the desulfurization (of SO_2) of flue gases resulted from the burning of BFG at its different

* Corresponding authors.
E-mail addresses: zhangaist@syuct.edu.cn (Z.-g. Zhang), ybcui@ipe.ac.cn (Y. Cui).

https://doi.org/10.1016/j.gee.2024.02.002

application sites, the desulfurization of BFG itself not only reduces the costs, but also avoids corrosion and environmental pollution. To make full use of the heat and pressure power generation from BFG, the desulfurization unit should be placed after the top recovery turbine (TRT) unit. Normally, the BFG pressure significantly decreases after TRT and the temperature drops from 150 °C to ca. 60 °C [7].

COS is usually converted into H_2S through catalytic hydrolysis and subsequently removed [8–12]. Thus, developing an efficient approach for H_2S removal is crucial to reduce the total sulfur content in BFG. Currently there have four technologies for H_2S removal, including adsorption, amine scrubbing, Claus process and selective catalytic oxidation [13–15]. Due to its easy operation, low cost and long service life, the adsorption method (especially solid adsorbent) is the most promising method, which is also convenient for practical application. The sulfur-containing gas after adsorption process can be piped to sintering furnace for combustion and then be disposed centralizedly. Therefore, solid adsorbents with high sulfur capacity and long service life is essential for effective H_2S removal from BFG.

Different zeolite (such as, natural zeolite, LTA zeolite, MFI and FAU zeolite) have been used for H_2S removal, and 13X zeolite demonstrates a good desulfurization performance [16–19]. However, the sulfur capacity of zeolite is relatively low and needs to improve. The addition of transition metal (such as Cu, Zn, Fe, Co, and Ag) on zeolite can enhance the sulfur capacity of zeolite-based adsorbents [20–26]. CuO is a potential candidate for low-temperature desulfurization due to its favorable thermodynamic properties [27–31]. Generally, active metal is loaded on zeolite via impregnation method in order to facilitate large-scale preparation. However, metal particles will agglomerate during calcination and large metal particles will form. The large metal particle may increase the gas diffusion resistance in adsorbent and inhibit the desulfurization performance [32–37]. Therefore, minimizing the metal particles on zeolite with a high loading is the key for the preparation of a high sulfur capacity adsorbent.

In present work, an ammonia-induced copper-modified 13X zeolite (NH_3–CuO/13X) adsorbent was prepared. By introducing ammonia, Cu^{2+} metal complexes can form and adsorbs on 13X zeolite during impregnation process and then be converted into CuO in subsequent calcination process. The amino groups effectively inhibit the agglomeration of CuO particles and therefore prevent the pores of zeolite from being blocked, which is certainly beneficial for the diffusion of H_2S in desulfurization process and hence capable of improving H_2S adsorption rate and sulfur capacity of adsorbent. The sulfur capacity of NH_3–CuO/13X-3 is more than twice that of CuO/13X (without ammonia introduced). In addition, ammonia induction was also successfully applied to the preparation of other kind of zeolite adsorbents. It was found that the performance of these adsorbents was also significantly improved, indicating the versatility of the induction of amino groups for the preparation of H_2S adsorbents via impregnation method.

2. Experimental section

2.1. Preparation of sorbent

Materials: The 13X zeolite is a commercial material (powder, Si/Al = 1.13, 2~3 μm, Jiangxi Xintao Technology Instrument Co., Ltd.), and the element content of 13X zeolite was shown in Table S1. Copper nitrate ($Cu(NO_3)_2 \cdot 3H_2O$, 99 %) was purchased from Xilong Chemical Co., Ltd. Ammonia ($NH_3 \cdot H_2O$) was obtained from Guoyao Chemical Reagent Co., Ltd. All reagents were of analytical grade and used as received from the suppliers without further purification.

Synthesis of adsorbents: All tested adsorbents were prepared using an improved impregnation method, as illustrated in Fig. 1a. Initially, 5.6 g of copper nitrate was dissolved in 80 mL of water under ultrasound to form a homogeneous solution. Then, $NH_3 \cdot H_2O$ was added dropwise into the solution under a vigorous stirring condition until the precipitate dissolves to form a stable blue tetra-ammonium copper complex ion. Subsequently, 10 g of 13X zeolite was added to the above solution and the mixture was stirred for 12 h. After stirring, the mixture was evaporated in a water bath at 80 °C and dried in an oven at 105 °C. Finally, the dried sample was ground and calcined at 250 °C for 4 h in a muffle furnace, and the resulting sample was named NH_3–CuO/13X-3. It had a Cu loading of approximately 12.84 wt%. NH_3–CuO/13X-1, NH_3–CuO/13X-2 and NH_3–CuO/13X-4 were synthesized similarly with different mass ratios of 13X zeolite to copper nitrate (10:2.8, 10:4.2, and 10:7), resulting in Cu loadings of approximately 6.86 wt%, 9.95 wt%, and 15.55 wt%, respectively. CuO/13X and NH_3/13X adsorbents were prepared using the same method for comparison. Additionally, to verify the universality of this ammonia induction method, NH_3–CuO/NaX and CuO/NaX were prepared by the same procedure. After desulfurization tests, the spent adsorbents were labeled with "Ex" (e.g., NH_3–CuO/13X-3-Ex), and the corresponding regenerated adsorbents were labeled with "R" (e.g., NH_3–CuO/13X-3-R).

The methods used for the characterization of all adsorbents included XRD, H_2-TPR, BET, SEM, TEM, XPS, TG-DTG, ICP-OES and FTIR and the detail procedures are described in Supporting Information.

2.2. Adsorption experiments

The test system for the performance of adsorbents is depicted in Fig. S1 (Supporting Information). Typically, H_2S from a gas cylinder was diluted with a simulated BFG (CO_2 19.68 vol%, O_2 0.30 vol%, CH_4 0.50 vol%, H_2 4.49 vol%, CO 24.02 vol%, N_2 51.01 vol%) to required concentrations (C (H_2S): 300 ppm/417.18 mg m^{-3}). The total flow rate of the gas (Q) and the mass of adsorbent (m) were fixed at 100 mL min^{-1} and 0.65 g (30–50 mesh granules were prepared by pressing tablets and sieving), which corresponded to a gas volume space velocity (GHSV) of 6000 h^{-1}. The H_2S adsorption

Please cite this article as: E. Cao et al., Ammonia-induced CuO/13X for H_2S removal from simulated blast furnace gas at low temperature, Green Energy & Environment, https://doi.org/10.1016/j.gee.2024.02.002

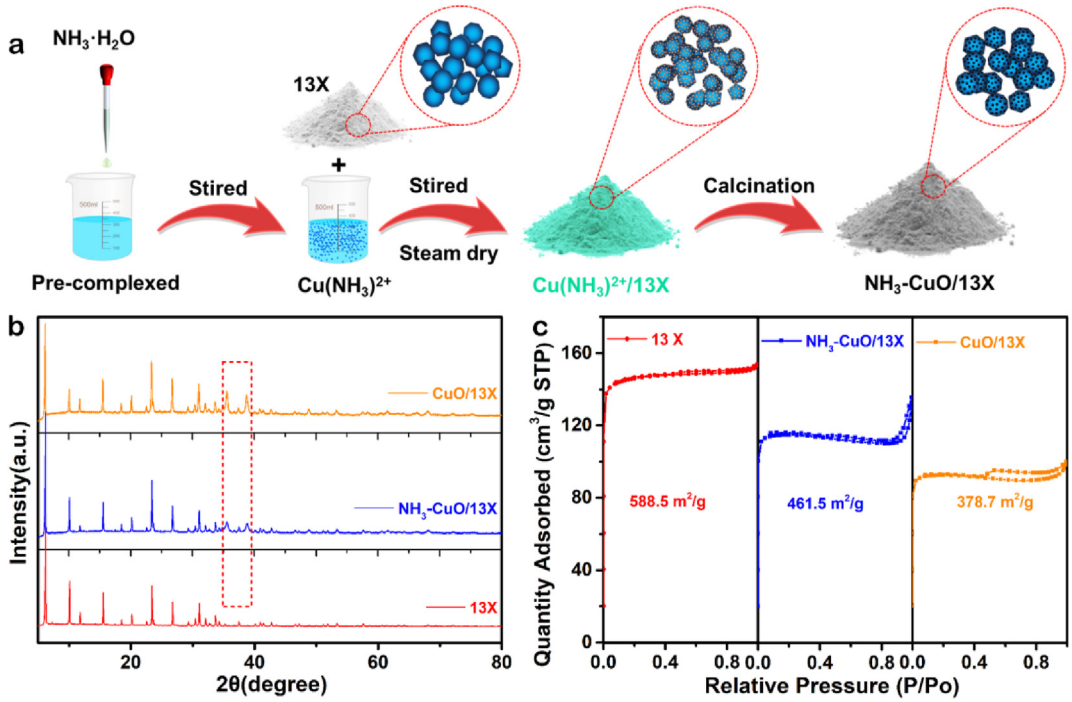

Fig. 1. (a) Schematic illustration for the synthesis of NH_3–CuO/13X. (b) XRD patterns and (c) N_2 adsorption/desorption isotherms of 13X, NH_3–CuO/13X-3 and CuO/13X.

performance of the adsorbent with water vapor was studied by introducing a certain amount of water vapor into the reactor through branch dilution gas. The temperature of the water vapor generator was kept at 60 °C, and the water vapor was introduced into the reactor through 8 mL min^{-1} branch dilution gas. The total water vapor content was 1.6 vol%.

The temperature (T) for adsorption was set within the range of 20 °C–80 °C. The H_2S concentration in the outlet gas was measured by a SP-6802 trace sulfur gas chromatograph (Shandong Lunanhongrui Chemical Instrument Co., Ltd., China), equipped with a flame photometric detector (FPD). The FPD detector temperature was set at 120 °C. The H_2S concentration was measured until the concentration of H_2S in outlet gas reached 15 ppm, that is, the penetration rate reached 5%. This threshold was used to catalculate the breakthrough sulfur capacity of all adsorbants. The exhaust gas is passed into $KMnO_4$ solution to mitigate its environmental impact.

Concretely, the breakthrough H_2S capacity of adsorbents was calculated by integrating the area of the breakthrough curve using equation (1):

$$H_2S\ \text{capacity}\ \left(\text{mg g}^{-1}\right) = \frac{M_{H_2S} \times V \times C_{in}}{m_0 \times 22.4} \int_0^t \left[1 - \frac{C_{out}}{C_{in}}\right] dt \quad (1)$$

where M_{H2S} is the molar mass of H_2S gas (34 g mol^{-1}), m_0 is the initial mass of fresh adsorbents (0.65 g), V is the total flow rate (100 mL min^{-1}), 22.4 is the volume of gas per mole (L mol^{-1}) at 0 °C, C_{in} is the H_2S concentration (ppm) in inlet gas, C_{out} is the H_2S concentration (ppm) in outlet gas, and t represents the desulfurization test time (min).

2.3. Regeneration of adsorbent

The regeneration experiments of the spent adsorbents were carried out at 200 °C under different atmospheres (simulated BFG or air) and GHSV of 600 h^{-1}. Once there was no sulfur-containing species to be detected from exhaust gas, the sample was naturally cooled down to room temperature.

3. Results and discussion

3.1. Characterization of adsorbents

XRD measurements were performed to identify the phase composition and crystallographic structure of adsorbents (13X, NH_3–CuO/13X-3 and CuO/13X). As the NH_3–CuO/13X-3 adsorbent had the highest H_2S adsorption performance among difference NH_3–CuO/13X (see Section 3.2), it was preferentially subjected to characterization. A series of typical characteristic peaks (Fig. 1b and Fig. S2) ascribed to 13X (2θ = 6.1, 10.0, 11.7, 15.4, 23.2, 26.6, 30.4, 31.0, 32.1 and 33.7°, PDF#89–8235) were observed for all samples [13,38], suggesting that the loading of Cu does not significantly change the crystal structure of 13X. Typical characteristic diffraction peaks assigned to CuO were detected for NH_3–CuO/13X-3 and CuO/13X samples (2θ = 32.5, 35.4, 38.9, 48.8, 58.2, and 61.3°, PDF#48–1548) [39,40]. No other Cu-related diffraction peaks were found, indicating that the precursor copper complex was completely converted into CuO after calcination. The full width at half maxima (FWHM) of CuO diffraction peak for NH_3–CuO/13X-3 was larger than that of CuO for CuO/13X, indicating the formation of smaller CuO particles in

Please cite this article as: E. Cao et al., Ammonia-induced CuO/13X for H_2S removal from simulated blast furnace gas at low temperature, Green Energy & Environment, https://doi.org/10.1016/j.gee.2024.02.002

NH_3–CuO/13X-3. Calculated by Scherrer's equation, the diameters of CuO nanoparticles in NH_3–CuO/13X-3 and CuO/13X-3 are 4.92 nm and 5.83 nm, respectively. The NH_3–CuO/13X-3 and CuO/13X were also analyzed by H_2-TPR, and the results are presented in Fig. S3. The main reduction peak at 215 °C can be attributed to the reduction of small CuO nanoclusters to Cu^0, and the peak centered at 266 °C be assigned to the reduction of large CuO particles to Cu^0 [41–43]. Compared with CuO/13X, NH_3–CuO/13X-3 has a peak at 215 °C with a larger area, indicating that NH_3–CuO/13X-3 has more small CuO nanoclusters. It may be owing to the induction of ammonia, which increases the dispersion of CuO.

In order to confirm that the dispersion of Cu species on zeolite, 13X, NH_3–CuO/13X-3 and CuO/13X were subjected to N_2 adsorption/desorption isotherms measurement. The results are presented in Fig. 1c and Fig. S4. The high specific surface area of 13X zeolite can be attributed to its microporous structure. The specific surface areas of NH_3–CuO/13X-3 and CuO/13X decreased after Cu impregnation. The specific surface area of NH_3–CuO/13X-3 is higher (461.5 m^2 g^{-1}) than that of CuO/13X (378.7 m^2 g^{-1}). Pore size distribution analysis showed that the total pore volume of NH_3–CuO/13X-3 adsorbent decreased less after Cu loading compared with CuO/13X (Table S2). The reason may be that the introduction of ammonia inhibited the agglomeration of Cu particles and reduces the blockage of the pores of 13X zeolite and allowed more N_2 molecules to enter the channels. Preservation of more accessible channels certainly favors the reduction of gas diffusion resistance [34], and therefore is beneficial to the diffusion of H_2S in adsorbent.

SEM images in Fig. S5 illustrate that the surface of 13X changes from smooth to rough after Cu impregnation. As can be seen from the TEM images of NH_3–CuO/13X-3 and CuO/13X (Fig. 2a and b and S6), a large number of Cu nanoparticles are scattered on the surface of 13X. The average particle diameter of Cu in NH_3–CuO/13X-3 is 5.01 nm (Fig. 2b), which is smaller than that of Cu nanoparticles (5.75 nm) in CuO/13X (Fig. S6b). In Fig. 2c, the distinct lattice fringes with d spacing of 0.23 nm assigned to CuO (111) planes can be observed. The EDX analysis (Fig. 2d) indicated the Cu content on the surface of zeolite in NH_3–CuO/13X-3 is 11.69 wt%, which is close to the content of impregnated Cu (12.84 wt%), indicating that most of Cu on

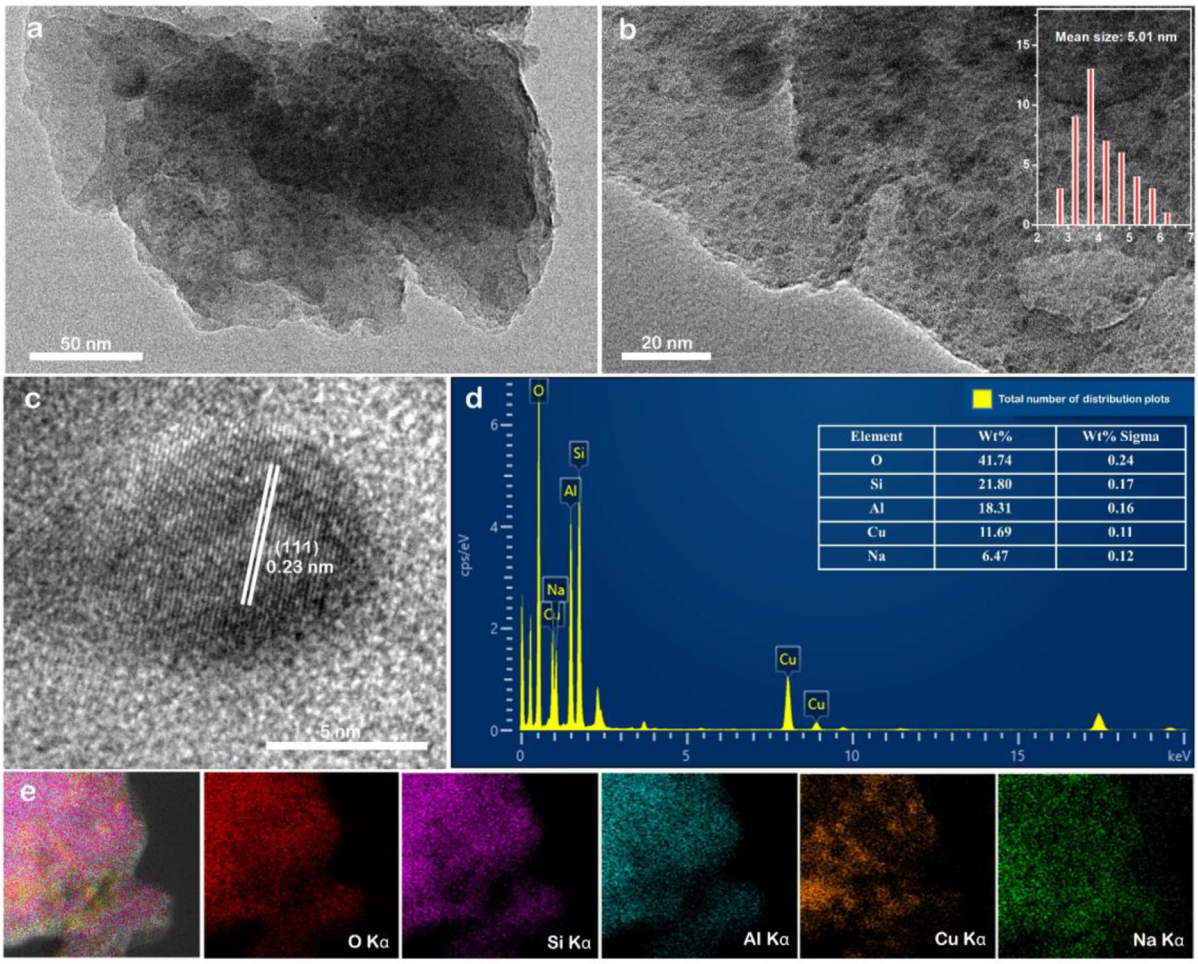

Fig. 2. (a-b) TEM images of NH_3–CuO/13X-3, (c) HRTEM image and (d-e) EDX elemental mapping images of NH_3–CuO/13X-3. The inset in (b) is the corresponding diameter distribution of CuO nanoparticles on 13X zeolite.

Please cite this article as: E. Cao et al., Ammonia-induced CuO/13X for H_2S removal from simulated blast furnace gas at low temperature, Green Energy & Environment, https://doi.org/10.1016/j.gee.2024.02.002

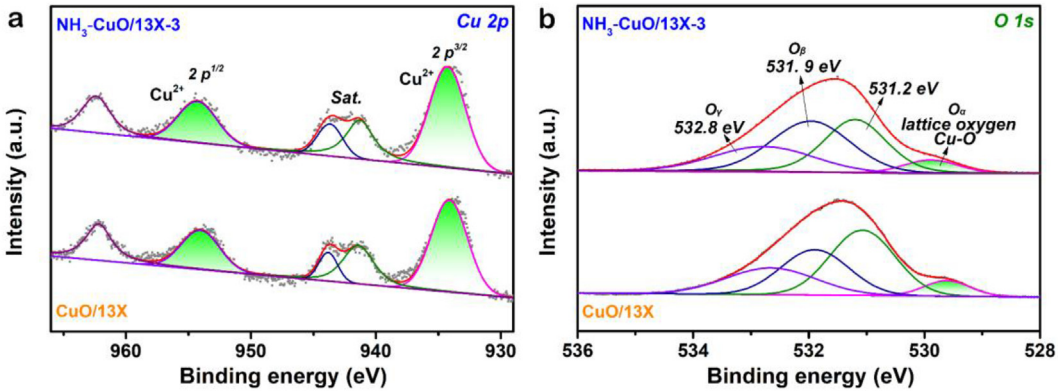

Fig. 3. (a) High-resolution Cu 2p spectra and (b) O 1s spectra of NH_3–CuO/13X-3 and CuO/13X.

the surface of 13X zeolite. Furthermore, the Cu content in NH_3–CuO/13X-3 adsorbent was measured by ICP-OES. The Cu content in NH_3–CuO/13X-3 is 12.83 wt%, which is close to the feeding amount. Besides, the other elements (O, Si, Al and Na) are also distributed uniformly within its framework (Fig. 2e).

The surface chemical and valence states of 13X, NH_3–CuO/13X-3 and CuO/13X were investigated by XPS (Fig. 3 and Fig. S7). The peaks attributed to Cu species appeared in the XPS spectra of NH_3–CuO/13X-3 and CuO/13X, in addition to Al, Si, Na and O signals (Fig. S7a). The valence states of Cu and O were investigated via high-resolution spectrum analysis. Fig. 3a shows the high-resolution Cu 2p core-level XPS spectra of NH_3–CuO/13X-3 and CuO/13X. It can be seen that the 2p spectra of Cu for two adsorbents are basically the same, indicating that the introduction of ammonia did not affect the valence state of Cu. The pair of peaks at 934.8 and 954.8 eV arising from the spin–orbit doublet of Cu 2p are indexed to Cu^{2+} [44,45]. The satellite peaks centered at 942.6 eV and 962.6 eV are also corresponds to Cu^{2+}. Fig. 3b shows the O 1s XPS spectra of NH_3–CuO/13X-3 and CuO/13X. Compared with the case of 13X (Fig. S7c), the oxygen in NH_3–CuO/13X-3 and CuO/13X has a distinct peak at 529.8 eV, which is corresponding to lattice oxygen (O_α) (Fig. 3b and Fig. S7d) [46]. Peaks centered at 531.9 eV and 532.8 eV can be assigned to chemically adsorbed oxygen (O_β) and adsorbed water (O_γ) [47], and the peak centered at 531.2 eV is attributed to oxygen in zeolite structure.

3.2. Adsorbents performance

The performance of different adsorbents for H_2S removal was evaluated in a quartz tube reactor at 80 °C. The breakthrough curves and breakthrough sulfur capacity of various adsorbents are presented in Fig. 4. For each adsorbent, H_2S adsorption performance gradually declined with desulfurization time and eventually the H_2S concentration in outlet gas reached the breakthrough point (>15 ppm, 5% penetration rate). The 13X zeolite have low capacity (1.9 mg g^{-1}) to remove H_2S completely and low breakthrough sulfur capacity (11.5 mg g^{-1}). The introduction of ammonia slightly enhances the performance of 13X zeolite. The complete removal and breakthrough sulfur capacities of NH_3/13X are 7.1 and 16.8 mg g^{-1}, respectively. Among the adsorbents, NH_3–CuO/13X-3 exhibited the highest capacity (63.8 mg g^{-1}) for the full removal of H_2S and the highest breakthrough sulfur capacity (74.4 mg g^{-1}), which is more than twice the values of CuO/13X (23.3 and 33.1 mg g^{-1}). It indicates that the H_2S adsorption performance of CuO-based adsorbents could been improved significantly via ammonia induction during the

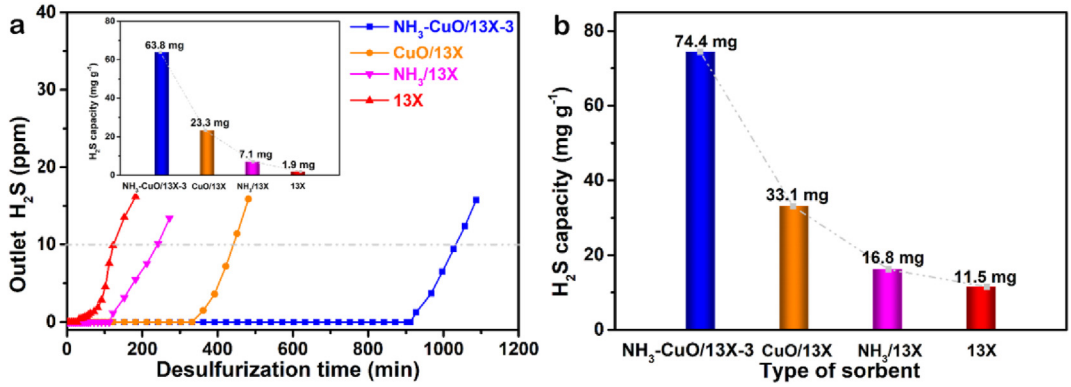

Fig. 4. (a) Breakthrough curves and (b) breakthrough sulfur capacity of NH_3-CuO/13X-3, CuO/13X, NH_3/13X and 13X. The inset in (a) is the sulfur capacity of different adsorbents to remove H_2S completely.

Please cite this article as: E. Cao et al., Ammonia-induced CuO/13X for H_2S removal from simulated blast furnace gas at low temperature, Green Energy & Environment, https://doi.org/10.1016/j.gee.2024.02.002

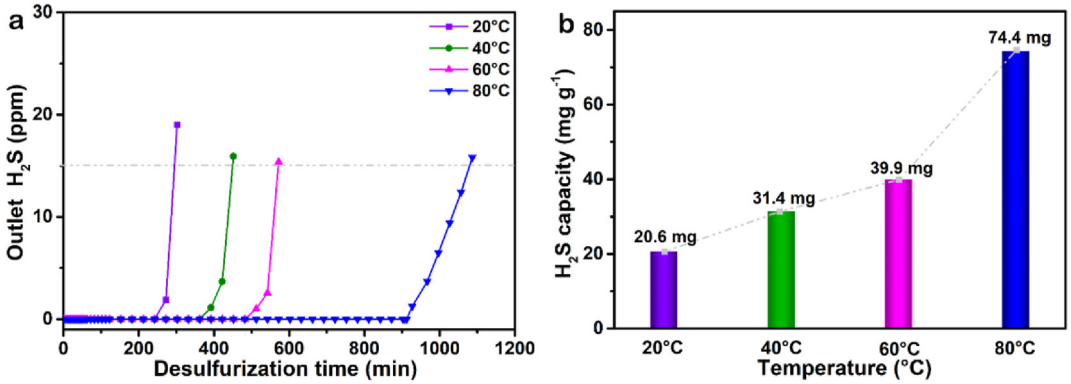

Fig. 5. (a) Breakthrough curves and (b) breakthrough sulfur capacity of NH_3–CuO/13X-3 adsorbent at different adsorbent temperatures.

impregnation process. The H_2S adsorption capacity of NH_3–CuO/13X-3 in our work exceeds most previously reported zeolite-related adsorbents (Table S3). The content of Cu in NH_3–CuO/13X has an effect on the performance of H_2S removal (Fig. S8). The breakthrough sulfur capacity of NH_3–CuO/13X was continuously improved when the content of Cu was increased from 6.86 to 12.84 wt%. However, the breakthrough sulfur capacity of NH_3–CuO/13X decreased when the content of Cu further increased to 15.55 wt%. That is, NH_3–CuO/13X-3 exhibited the highest H_2S removal performance among all tested NH_3–CuO/13X samples. Thus, NH_3–CuO/13X-3 was selected to further investigate the effect of calcination temperature on its sulfur capacity (Fig. S9). It can be seen from Fig. S9 that calcination temperature had no significant effect on the sulfur capacity of NH_3–CuO/13X-3, demonstrating that the adsorbent could exhibit high thermal stability and the induction of ammonia can effectively inhibit the agglomeration of metal particles at high temperature.

In order to study the effect of H_2S adsorbing temperature on the desulfurization performance, H_2S removal of NH_3–CuO/13X-3 was evaluated over a temperature range of 20–80 °C. As shown in Fig. 5, the performance of H_2S adsorption increased with the increase of H_2S adsorbing temperature. The H_2S removal capacities of NH_3–CuO/13X-3 at different adsorbing temperatures (20, 40, 60 and 80 °C) were 20.6, 31.4, 39.9 and 74.4 mg g^{-1}, respectively. This phenomenon can be explained since H_2S molecules may gain energy and overcome the kinetic limitation as the reaction temperature increasing [48,49]. The NH_3–CuO/13X-3 adsorbent exhibited the excellent desulfurization performances in low temperature range (less than 80 °C), demonstrating its suitability for H_2S removal from BFG at practical conditions.

Normally, the water vapor content of BFG after dust removal is ca. 1.6 vol%. Therefore, evaluation the H_2S removal performance of adsorbent in simulated BFG with water vapor becomes essential. The H_2S adsorbent performance of NH_3–CuO/13X-3 was tested in simulated BFG containing 1.6 vol% water vapor at 80 °C. The breakthrough curve and H_2S adsorption capacity are shown in Fig. 6. The introduction of water vapor in simulated BFG resulted in a measurable reduction of breakthrough time and H_2S adsorption capacity for NH_3–CuO/13X-3. It can be attributed to the competitive adsorption of H_2S and H_2O on the adsorbent due to similar structure and polarity of H_2S and H_2O molecules. Nevertheless, the breakthrough sulfur capacity of NH_3–CuO/13X-3 still maintained high at 56.7 mg g^{-1} with 1.6 vol% water vapor, demonstrating that this adsorbent is sufficiently effective for the desulfurization of realistic BFG.

To demonstrate the universality of the ammonia induction method for the preparation of highly-efficiency H_2S removal

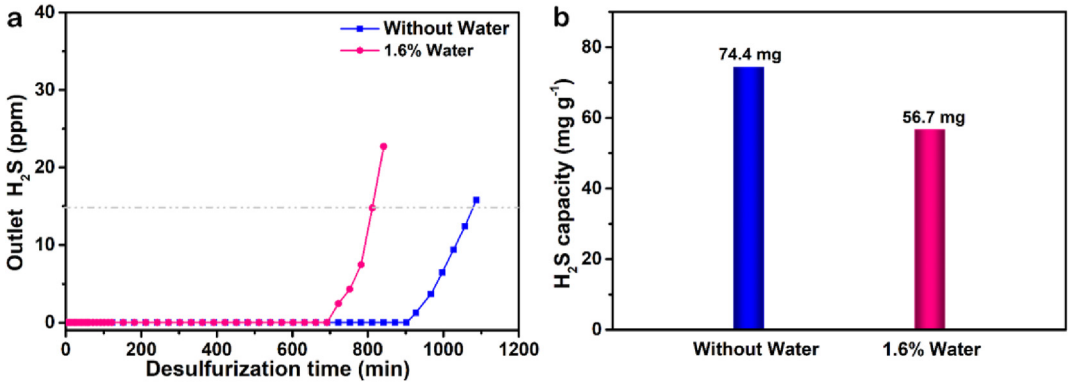

Fig. 6. (a) Breakthrough curves and (b) breakthrough sulfur capacity of NH_3–CuO/13X-3 adsorbent in simulated BFG with/without water.

Please cite this article as: E. Cao et al., Ammonia-induced CuO/13X for H_2S removal from simulated blast furnace gas at low temperature, Green Energy & Environment, https://doi.org/10.1016/j.gee.2024.02.002

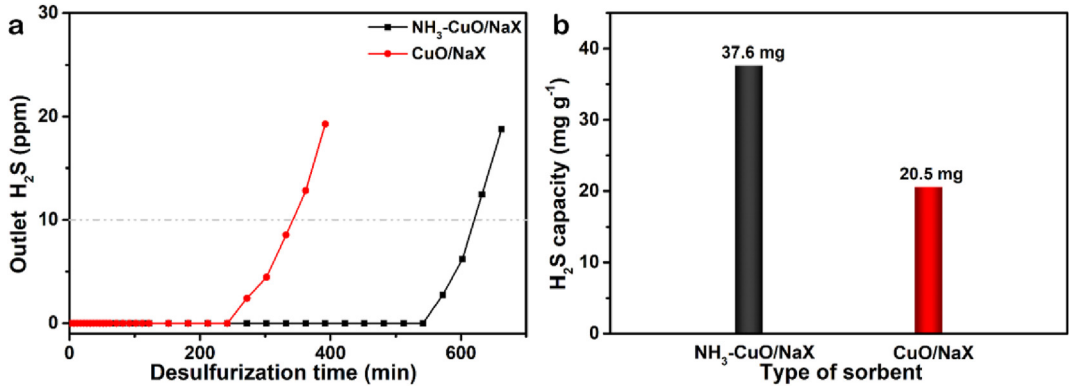

Fig. 7. (a) Breakthrough curves and (b) breakthrough sulfur capacity of NH_3–CuO/NaX and CuO/NaX.

adsorbent, two adsorbents based NaX zeolite (NH_3–CuO/NaX and CuO/NaX) were also prepared by the same procedure with ammonia induction (Fig. 7). Compared with CuO/NaX adsorbent (20.5 mg g^{-1}), the breakthrough sulfur capacity of NH_3–CuO/NaX was nearly doubled, reaching a level of 37.6 mg g^{-1}. It suggests that ammonia induction may offer a universal method for the preparation of H_2S adsorbents with high sulfur capacity via impregnation met hod.

3.3. Regeneration performance of NH_3–CuO/13X-3-Ex adsorbent

The thermogravimetric curve in air of used adsorbent (NH_3–CuO/13X-3-Ex) was presented in Fig. S10. The weight loss in temperature range of 46–200 °C should be attributed to the desorption of H_2O and H_2S adsorbed in the spent sample. The small weight increasement at 200–350 °C is possibly due to the formation of sulfur oxides such as SO_4^{-2}. Therefore, the regeneration of NH_3–CuO/13X-3-Ex was studied at 200 °C in air and then subjected to simulated BFG to evaluate its sulfur capacity (Fig. 8). The breakthrough capacity of the regenerated NH_3–CuO/13X-3 was 17.3 mg g^{-1} (Fig. 8a). After the second regeneration cycle, the sample became fully inert for H_2S adsorption, indicating that the regeneration of NH_3–CuO/13X-3-Ex in air is not viable. Fig. 8b presents the breakthrough curve and sulfur capacity of NH_3–CuO/13X-3-Ex regenerated in simulated BFG. The breakthrough sulfur capacity of NH_3–CuO/13X-3 after first regeneration cycle was 25.3 mg g^{-1}, and it still remained a relatively high level of 19.0 mg g^{-1} after second regeneration cycle. Clearly the breakthrough sulfur capacity of the adsorbent regenerated in simulated BFG has a smaller drop than that of the adsorbent regenerated in air. From the results of the specific surface area and pore size distribution of NH_3–CuO/13X-3-Ex and NH_3–CuO/13X-3-R after regeneration in BFG (Fig. S11), it can be seen that the specific surface area and pores of the adsorbent after regeneration in BFG have been well restored (Fig. 1c, S4 and S11). In addition, the regeneration of NH_3–CuO/13X-3-Ex at higher temperature (350 °C and 450 °C) was also carried out (Fig. S12). It can be seen that the sulfur capacity of NH_3–CuO/13X-3 after regeneration at higher temperature decreases, no matter in air or BFG.

3.4. Desulfurization mechanism of NH_3–CuO/13X-3 adsorbent

The FT-IR and XPS spectra of the spent adsorbents (NH_3–CuO/13X-3-Ex) were used to reveal the main reaction and deactivation mechanism. Compared with the FT-IR spectra of NH_3–CuO/13X-3 (Fig. 9a), a new band at 620 cm^{-1} appeared in the spectrum of NH_3–CuO/13X-3-Ex, which could be attributed to Cu–S vibration [46,50]. This indicates that copper sulfides formed in the spent sample.

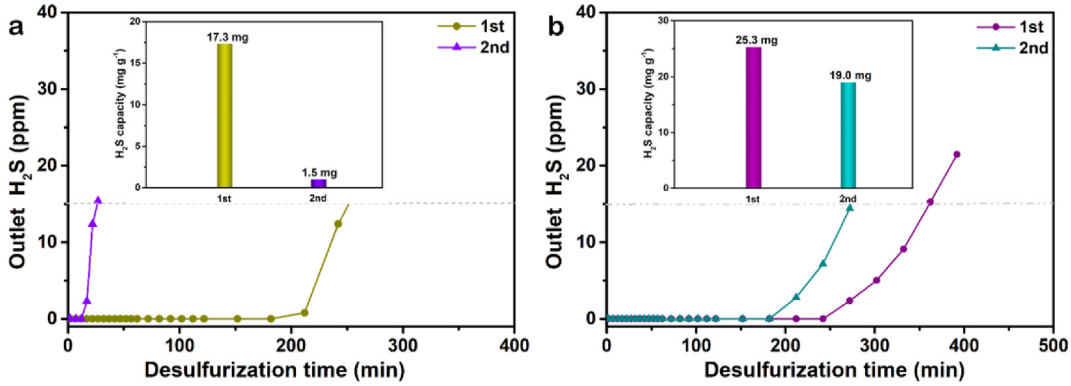

Fig. 8. Breakthrough curves and breakthrough sulfur capacity of NH_3–CuO/13X-3-Ex after regeneration in (a) air and (b) simulated BFG at 200 °C.

Please cite this article as: E. Cao et al., Ammonia-induced CuO/13X for H_2S removal from simulated blast furnace gas at low temperature, Green Energy & Environment, https://doi.org/10.1016/j.gee.2024.02.002

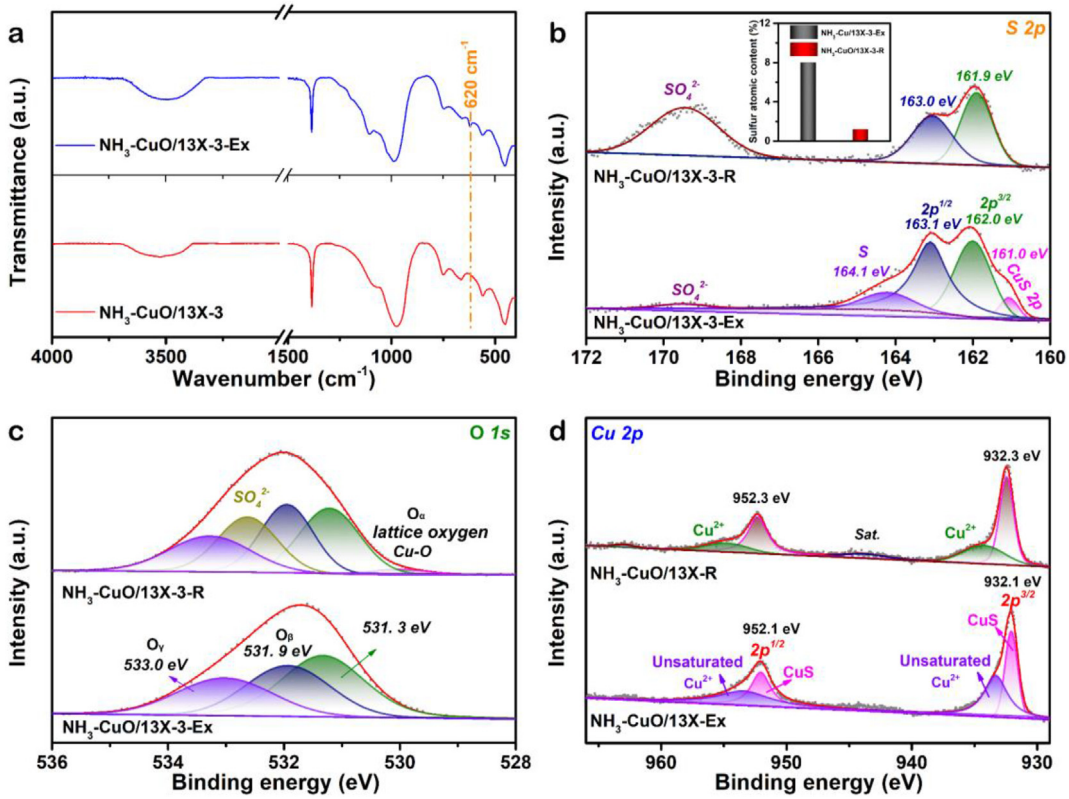

Fig. 9. (a) FT-IR spectra of NH_3–CuO/13X-3 and NH_3–CuO/13X-3-Ex; (b) High-resolution S 2p spectra of NH_3–CuO/13X-3-Ex and NH_3–CuO/13X-3-R, (c) High-resolution O 1s spectra of NH_3–CuO/13X-3-Ex and NH_3–CuO/13X-3-R, (d) Cu 2p spectra of NH_3–CuO/13X-3-Ex and NH_3–CuO/13X-3-R. The inset in (b) is a diagram of S content in NH_3–CuO/13X-3-Ex and NH_3–CuO/13X-3-R.

Fig. S13 and Fig. 9b-9d present the XPS spectra of NH_3–CuO/13X-3-Ex. The XPS spectra of NH_3–CuO/13X-3-Ex (Fig. S13) confirmed the co-presence of Al, Si, Na, Cu, S and O elements. The XPS S 2p spectrum of NH_3–CuO/13X-3-Ex (Fig. 9b) can be fitted with five peaks. The three peaks centered at 161.0 eV (S 2p), 162.0 eV (S 2p3/2) and 163.1 eV (S 2p1/2) are attributed to the standard binding energy of metal sulfide (CuS) [44,51]. The two peaks centered at 164.1 eV and 169.4 eV are ascribed to S and sulfate, respectively [52,53]. The formation of S and sulfate may be due to the catalytic oxidation of adsorbed H_2S co-promoted by 13X zeolite and CuO. The framework of 13X is similar to that of γ-Al_2O_3, which is a common catalyst used in Claus process to covert H_2S into S [38]. In order to verify this, XPS analysis was performed for the H_2S-adsorbed 13X zeolite (Fig. S14). The sulfur components did exist in the forms of S and sulfate, which is consistent with results reported in literature [38]. By comparing the XPS peak areas related to sulfur, it was found that the sulfur species in NH_3–CuO/13X-3-Ex are mainly present as CuS (Fig. 9b). As shown in Fig. 9c, the O 1s XPS spectrum of NH_3–CuO/13X-3-Ex can be deconvoluted oxygen in zeolite structure (531.3 eV), chemical adsorbed oxygen (531.9 eV, O_β) and adsorbed H_2O (533.0 eV, O_γ), respectively. Compared with NH_3–CuO/13X-3, the signal of lattice oxygen (O_α) of NH_3–CuO/13X-3-Ex is not detectable, suggesting that no Cu in the NH_3–CuO/13X-3-Ex existed in the form of CuO. For confirmation, Cu 2p XPS spectrum of NH_3–CuO/13X-3-Ex is given in Fig. 9d. No CuO peak is observed, and the two peaks centered at 932.1 eV and 952.1 eV are attributed to a coordination of unsaturated Cu^{2+} and CuS, respectively [54].

Since the better regeneration performance of NH_3–CuO/13X-3-Ex was achieved in the simulate BFG, XPS analysis was conducted for NH_3–CuO/13X-3-R regenerated in simulate BFG to explore the regeneration mechanism. The XPS spectra of NH_3–Cu/13X-3-R confirmed the presence of Al, Si, Na, Cu, S, and O elements (Fig. S13). The S content in NH_3–CuO/13X-3 before and after regeneration was 8.0% and 1.2% (Fig. 9b), indicating that most of sulfur was removed after regeneration. The XPS of S 2p spectrum for NH_3–CuO/13X-3-R (Fig. 9b) can be fitted with three peaks centered at 161.9 eV (S 2p3/2), 163.0 eV (S 2p1/2) and 169.4 eV (SO_4^{2-}). The former two peaks are attributed to non-regenerated CuS or Cu_2S produced in the regeneration process [55]. The peaks centered at 169.4 eV is ascribed to sulfate. The peak intensity attributable to SO_4^{2-} has increased after regeneration, and most of sulfur in CuS has been removed, resulting in an increase in the relative intensity of SO_4^{2-}. The XPS spectrum of O 1s for NH_3–CuO/13X-3-R (Fig. 9c) can be fitted into five peaks, corresponding to oxygen in zeolite structure (531.3 eV), chemisorbed oxygen (531.9 eV, O_β), adsorbed H_2O (533.0 eV, O_γ), SO_4^{2-} (532.5 eV), and lattice oxygen (529.8 eV, O_α). The presence of lattice oxygen confirms the formation of CuO. The Cu 2p XPS spectrum of NH_3–CuO/13X-3-R (Fig. 9d) exhibits obvious Cu^{2+} peaks, indicating

Please cite this article as: E. Cao et al., Ammonia-induced CuO/13X for H_2S removal from simulated blast furnace gas at low temperature, Green Energy & Environment, https://doi.org/10.1016/j.gee.2024.02.002

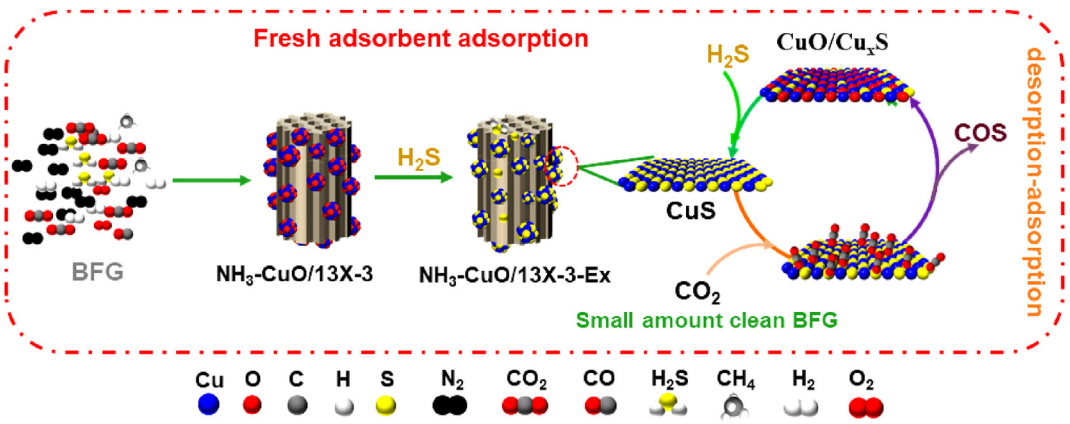

Fig. 10. H_2S removal and regeneration mechanism of NH3–CuO/13X-3 adsorbent.

that CuS was converted into CuO during the regeneration process. Via in-situ analysis of the exhaust gas, COS was detected during the regeneration of NH_3–CuO/13X-3 in simulate BFG over 150 °C. As BFG contains CO, S will react with CO to generate COS. In order to determine the formation of COS during the regeneration process, NH_3–CuO/13X-3-Ex adsorbent was regenerated by 24 vol% CO/N_2. It was found that only a small amount of COS was formed during the regeneration process. In addition, the performance of NH_3–CuO/13X-3-Ex after CO regeneration was also carried out (Fig. S15). It can be seen that the breakthrough sulfur capacity of NH_3–CuO/13X-3-Ex regenerated by CO is only 6.1 mg g^{-1}, which is far lower than that of NH_3–CuO/13X-3-Ex regenerated by simulated BFG, indicating that COS mainly comes from the reaction between CuS and CO_2. It proves that CuS was converted into CuO and COS in the regeneration process with CO_2-containing simulated BFG, which is consistent with the report in literature [32]. After adsorption of H_2S onto NH_3–CuO/13X-3-R-Ex, the peaks of CuO in XPS spectra disappeared and the peaks corresponding to unsaturated Cu^{2+} emerged (Fig. S16), indicating that the CuO formed during regeneration process served as active site for H_2S adsorption.

Based on above analysis and reported literature [32,38,44,56], the possible H_2S adsorption and regeneration mechanism over NH_3–CuO/13X-3 is shown in Fig. 10. For the fresh adsorbent, its main adsorption site is CuO, and the possible adsorption processes are as follows:

$$H_2S_{(g)} \rightarrow H_2S_{(ads)} \quad (2)$$

$$H_2S_{(ads)} + CuO \rightarrow CuO + HS^-_{(ads)} + H^+ \quad (3)$$

$$CuO + HS^-_{(ads)} \rightarrow CuO + S^{2-}_{(ads)} + H^+ \quad (4)$$

$$CuO + S^{2-}_{(ads)} \rightarrow CuS + O^{2-} \quad (5)$$

$$O^{2-} + 2H^+ \rightarrow H_2O \quad (6)$$

Due to the presence of adsorbed oxygen, partial catalytic oxidation of H_2S occurs, and the possible oxidation process is given below:

$$H_2S_{(ads)} + O^*_{(ads)} \rightarrow S_{(ads)} + H_2O_{(ads)} \quad (7)$$

The main reactions that occur during regeneration involve the reaction of CuS and CO_2 to form CuO and COS, and the possible desorption process is as follows:

$$CuS + CO_{2(g)} \rightarrow CuO + COS_{(g)} \quad (8)$$

4. Conclusions

In brief, a high-performance H_2S adsorbent (NH_3–CuO/13X) is successfully prepared by simple and low-cost impregnation method with ammonia-induced. The introduction of ammonia inhibits the agglomeration of Cu particles and the average particle diameter of Cu in NH_3–CuO/13X-3 is smaller than that of Cu nanoparticles in CuO/13X, which not only improves the dispersion of CuO (the active site for H_2S adsorption), but also inhibits the blockage of zeolite pores. The latter effect is beneficial to the diffusion of H_2S in adsorbent. For the simulated BFG with 300 ppm H_2S and at 80 °C, the NH_3–CuO/13X adsorbent exhibits a H_2S removal rate close to 100% and maintains for over 900 min. The breakthrough sulfur capacity of NH_3–CuO/13X reaches 74.4 mg g^{-1}, which is more than double that of CuO/13X prepared without NH_3 induction and surpasses most reported adsorbents. The enhanced desulfurization performance of NH_3–CuO/13X is attributed to the abundant pore of 13X and good dispersion of CuO. Ammonia induction offer a versatile method for the preparation of zeolite-based adsorbents with an enhanced sulfur capacity.

CRediT authorship contribution statement

Erping Cao: Writing – original draft, Methodology, Investigation, Funding acquisition, Formal analysis, Data curation. **Yuhua Zheng:** Writing – review & editing. **Hao Zhang:** Data curation. **Jianshan Wang:** Validation. **Yuran**

Please cite this article as: E. Cao et al., Ammonia-induced CuO/13X for H_2S removal from simulated blast furnace gas at low temperature, Green Energy & Environment, https://doi.org/10.1016/j.gee.2024.02.002

Li: Validation. **Tingyu Zhu:** Validation. **Zhan-guo Zhang:** Writing − review & editing. **Guangwen Xu:** Validation. **Yanbin Cui:** Writing − review & editing, Visualization, Project administration, Funding acquisition.

Conflict of interest

The authors declare that they have no known competing financial interests or personal relationships that could have appeared to influence the work reported in this paper.

Acknowledgment

This study is financially supported by National Natural Science Foundation of China (Grant. 22076189), National Key Research and Development Program of China (No. 2023YFC3707003), and the Joint Fund of Yulin University and Dalian National Laboratory for Clean Energy (Grant. YLU-DNL Fund 2022003).

Appendix A. Supplementary data

Supplementary data to this article can be found online at https://doi.org/10.1016/j.gee.2024.02.002.

References

[1] S.D. Angeli, S. Gossler, S. Lichtenberg, G. Kass, A.K. Agrawal, M. Valerius, K.P. Kinzel, O. Deutschmann, Angew. Chem. Int. Ed. 60 (2021) 11852−11857.
[2] A.A. Ramirez-Santos, C. Castel, E. Favre, Sep. Purif. Technol. 194 (2018) 425−442.
[3] M. Ma, C. Li, Y. Li, C. Wang, S. Gao, H. Ye, J. Li, J. Yu, Energy Fuels 36 (2022) 4837−4846.
[4] Y.Q. Zhang, Z.B. Xiao, J.X. Ma, Appl. Catal. B Environ. 48 (2004) 57−63.
[5] G. Guo, H. Guo, F. Wang, Liam. France, W. Yang, Z. Mei, Y. Yu, Green Energy Environ. 5 (2020) 114−120.
[6] H. Wang, H. Yi, P. Ning, X. Tang, L. Yu, D. He, S. Zhao, Chem. Eng. J. 166 (2011) 99−104.
[7] P.F. Li, G.C. Wang, Y. Dong, Y.Q. Zhuo, Y.M. Fan, Curr. Pollut. Rep. 8 (2022) 189−200.
[8] G. Mu, Y. Zeng, Y. Zheng, Y. Cao, F. Liu, S. Liang, Y. Zhan, L. Jiang, Green Energy Environ. 8 (2023) 831−841.
[9] B.P. Williams, N.C. Young, J. West, C. Rhodes, G.J. Hutchings, Catal. Today 49 (1999) 99−104.
[10] Y. Wang, L. Ding, H. Long, J. Xiao, L. Qian, H. Wang, C. Xu, Chemosphere 307 (2022) 136090.
[11] Y. Wang, X. Wu, D. Wei, Y. Chen, J. Yang, L. Wu, RSC Adv. 13 (2023) 12618−12633.
[12] Y. Liu, P. Wu, K. Shen, Y. Zhang, G. Li, B. Li, ACS Omega 7 (2022) 13299−13312.
[13] Y. Guo, B. Xiang, B. Zhao, W. Wang, Y. Xiang, J. Liao, L. Chang, J. Ma, W. Bao, Fuel 338 (2023) 127261.
[14] F. Kamali, M.M. Eskandari, A. Rashidi, M. Baghalha, M. Hassanisadi, T. Hamzehlouyan, J. Hazard Mater. 364 (2019) 218−226.
[15] X. Zheng, Y. Li, L. Zhang, L. Shen, Y. Xiao, Y. Zhang, C. Au, L. Jiang, Appl. Catal. B Environ. 252 (2019) 98−110.
[16] M. Ozekmekci, G. Salkic, M.F. Fellah, Fuel Process. Technol. 139 (2015) 49−60.
[17] A. Alonso-Vicario, J.R. Ochoa-Gomez, S. Gil-Rio, O. Gomez-Jimenez-Aberasturi, C.A. Ramirez-Lopez, J. Torrecilla-Soria, A. Dominguez, Microporous Mesoporous Mater. 134 (2010) 100−107.
[18] R. Dehghan, M. Anbia, Fuel Process. Technol. 167 (2017) 99−116.
[19] M.M. Tomadakis, H.H. Heck, M.E. Jubran, K. Al-Harthi, Sep. Sci. Technol. 46 (2011) 428−433.
[20] X. Xu, G. Huang, S. Qi, Chem. Eng. J. 316 (2017) 563−572.
[21] M.S. Shah, M. Tsapatsis, J.I. Siepmann, Chem. Rev. 117 (2017) 9755−9803.
[22] H. Yang, B. Tatarchuk, AIChE J. 56 (2010) 2898−2904.
[23] B. Elyassi, Y. Al Wahedi, N. Rajabbeigi, P. Kumar, J.S. Jeong, X. Zhang, P. Kumar, V.V. Balasubramanian, M.S. Katsiotis, K.A. Mkhoyan, N. Boukos, S. Al Hashimi, M. Tsapatsis, Microporous Mesoporous Mater. 190 (2014) 152−155.
[24] D. Montes, E. Tocuyo, E. Gonzalez, D. Rodriguez, R. Solano, R. Atencio, M.A. Ramos, A. Moronta, Microporous Mesoporous Mater. 168 (2013) 111−120.
[25] M. Hussain, N. Abbas, D. Fino, N. Russo, Chem. Eng. J. 188 (2012) 222−232.
[26] X. Wang, T. Sun, J. Yang, L. Zhao, J. Jia, Chem. Eng. J. 142 (2008) 48−55.
[27] D. Kim, D. Bae, Y.J. Kim, S.J. Lee, J.W. Lee, Y. Yun, N.K. Park, M. Kim, Appl. Sci. 11 (2021) 7775.
[28] J. Abbasian, R.B. Slimane, Ind. Eng. Chem. Res. 37 (1998) 2775−2782.
[29] M.H. Morcali, B. Zeytuncu, A. Baysal, S. Akman, O. Yucel, J. Environ. Chem. Eng. 2 (2014) 1655−1662.
[30] Y. Wang, F.H. Yang, R.T. Yang, J.M. Heinzel, A.D. Nickens, Ind. Eng. Chem. Res. 45 (2006) 7649−7655.
[31] S. Liu, B.O. Zhang, Z. Bai, F. Chen, F. Xie, J. Zhou, Y. Lu, G. Miao, J. Jin, Z. Zhang, Energy Fuels 32 (12) (2018) 13004−13014.
[32] D. Liu, S. Chen, X. Fei, C. Huang, Y. Zhang, Ind. Eng. Chem. Res. 54 (2015) 3556−3562.
[33] J. Shen, J. Zhou, N.G.C. Astrath, T. Navessin, Z.S. Liu, C. Lei, J.H. Rohling, D. Bessarabov, S. Knights, S. Ye, J. Power Sources 196 (2011) 674−678.
[34] K. Polychronopoulou, J.L.G. Fierro, A.M. Efstathiou, Appl. Catal. B Environ. 57 (2) (2005) 125−137.
[35] J. Jiao, J. Cao, Y. Xia, L. Zhao, Chem. Eng. J. 306 (2016) 9−16.
[36] Z. Zhao, X. Cui, J. Ma, R. Li, Int. J. Greenhouse Gas Control 1 (2007) 355−359.
[37] G.B. Baur, I. Yuranov, L. Kiwi-Minsker, Catal. Today 249 (2015) 252−258.
[38] K. Yang, B. Su, L. Shi, H. Wang, Q. Cui, Energy Fuel. 32 (2018) 12742−12749.
[39] H. Zhang, J. Wang, T. Liu, M. Zhang, L. Hao, T. Phoutthavong, P. Liang, Chem. Eng. J. 426 (2021) 131286.
[40] M. Balsamo, S. Cimino, G. de Falco, A. Erto, L. Lisi, Chem. Eng. J. 304 (2016) 399−407.
[41] J. Feng, F. Wang, C. Wang, K. Li, P. Ning, X. Sun, L. Jia, Sep. Purif. Technol. 277 (2021) 119420.
[42] Y. Wang, Q. Ying, Y. Zhang, Y. Liu, Z. Wu, Appl. Catal., A 590 (2020) 117373.
[43] U.R. Pillai, S. Deevi, Appl. Catal. B Environ. 64 (2006) 146−151.
[44] J. Feng, L. Jia, F. Wang, X. Sun, P. Ning, C. Wang, Y. Li, K. Li, Chem. Eng. J. 451 (2023) 138815.
[45] X. Du, J. Huang, Y. Feng, Y. Ding, Chin. J. Catal. 37 (2016) 123−134.
[46] S. Liang, B. Peng, S. Liu, W. Zhang, M. Guo, F. Cheng, M. Zhang, Environ. Sci. Technol. 54 (2020) 5964−5972.
[47] X. Zhang, S. Xiang, Q. Du, F. Bi, K. Xie, L. Wang, Mol. Catal. 522 (2022) 112226.
[48] F. Yazdanbakhsh, M. Blaesing, J.A. Sawada, S. Rezaei, M. Mueller, S. Baumann, S.M. Kuznicki, Ind. Eng. Chem. Res. 53 (2014) 11734−11739.
[49] X. Wang, J. Chong, S. Liang, M. Guo, M. Zhang, Fuel 334 (2023) 126546.
[50] M. Khabazipour, M. Anbia, Ind. Eng. Chem. Res. 58 (2019) 22133−22164.
[51] G. Huang, E. He, Z. Wang, H. Fan, J. Shangguan, E. Croiset, Z. Chen, Ind. Eng. Chem. Res. 54 (2015) 8469−8478.

Please cite this article as: E. Cao et al., Ammonia-induced CuO/13X for H_2S removal from simulated blast furnace gas at low temperature, Green Energy & Environment, https://doi.org/10.1016/j.gee.2024.02.002

[52] J.A. Cecilia, M.D. Soriano, L. Marques Correia, E. Rodriguez-Castellon, J.M. Lopez-Nieto, R. Silveira Vieira, Microporous Mesoporous Mater. 294 (2020) 109875.
[53] C. Yang, M. Florent, G. de Falco, H. Fan, T.J. Bandosz, Chem. Eng. J. 394 (2020) 124906.
[54] H. Liang, W. Shuang, Y. Zhang, S. Chao, H. Han, X. Wang, H. Zhang, L. Yang, Chemelectrochem 5 (2018) 494–500.
[55] D.L. Perry, J.A. Taylor, J. Mater. Sci. Lett. 5 (1986) 384–386.
[56] K.J. Ko, H. Kim, Y.H. Cho, K.M. Kim, C.H. Lee, Sep. Purif. Technol. 305 (2023) 122539.

Please cite this article as: E. Cao et al., Ammonia-induced CuO/13X for H_2S removal from simulated blast furnace gas at low temperature, Green Energy & Environment, https://doi.org/10.1016/j.gee.2024.02.002